Journal of
Nanoscience and Nanotechnology
Vol. 13, 3360–3364, 2013

Analysis of Annealing Process on P3HT:PCBM-Based Polymer Solar Cells Using Optical and Impedance Spectroscopy

Jun Young Kim[1], Seunguk Noh[1], Jeonghun Kwak[2,*], and Changhee Lee[1,*]

[1] *Department of Electrical and Computer Engineering, Inter-University Semiconductor Research Center, Seoul National University, Seoul 151-744, Republic of Korea*
[2] *Department of Electronic Engineering, Dong-A University, Busan 604-714, Republic of Korea*

Thermal annealing is a well-known process for polymer solar cells because it improves the device characteristics. Especially, the carrier mobility and the light absorption of P3HT:PCBM are significantly improved after the annealing process. Here, we examined the changes in the morphology of P3HT:PCBM film according to the annealing temperature to find the changes during the thermal annealing process by measuring the optical absorption and X-ray diffraction. We also investigated the effect of two different annealing process (pre- and post-annealing) on the device performance of the standard polymer solar cells consisting of ITO/MoO_3 (10 nm)/P3HT:PCBM (150 nm)/LiF (0.5 nm)/Al (100 nm) by measuring current density–voltage and impedance characteristics. From the results, we found that the improvement in terms of the power conversion efficiency of the post-annealed device originated from the decrease of injection resistance between P3HT:PCBM layer and Al electrodes.

Keywords: Polymer Solar Cell, P3HT:PCBM, Thermal Annealing, Impedance Spectroscopy.

RESEARCH ARTICLE

1. INTRODUCTION

Organic solar cells as a renewable energy source have many advantages such as low cost, light weight, simple solution processes and mechanical flexibilit.[1–3] Although organic materials have short exciton diffusion length and low carrier mobility compared to inorganic materials, the power conversion efficiency (PCE) of organic solar cells has been improved up to 8% through the understanding of photophysics synthesis of new organic materials, and optimization of device structures.[4–6] Considering fast improvement so far and multifarious efforts of researchers, it is expected that the power conversion efficiency of 10%, desired for commercialization, can be achieved in the near future.[7]

In order to obtain higher device performance of organic solar cells, thermal annealing process is commonly employed in bulk heterojunction organic solar cells.[8–13] Thermal annealing process can increase the crystallinity of polymers and the light absorption, improve the nanoscale interpenetrating network of donors and acceptors and reduce the series resistance of the devices.[8] Although it is well-known that thermal annealing enhances the solar cell performances, there still exists an argument about the annealing procedure, i.e., pre- and post-annealing meaning that thermal treatment before and after depositing LiF/Al electrodes, respectively. Depending on the experimental conditions, some experimental results show better performance with pre-annealing, and other results indicate that post-annealing leads to better performance.[9–12] In addition, there are some reports showing that the devices treated with pre- and post-annealing exhibit similar device performances.[13]

In this study, we examined the changes in the active layer by measuring the optical absorption spectra and X-ray diffraction patterns for various annealing temperature, and investigated the effect of different annealing process on the device performance of prototypical polymer solar cells consisted of poly(3-hexylthiopene) (P3HT): phenyl-C61-butyric acid methyl ester (PCBM) active layer. We also studied the current density–voltage characteristics and impedance spectra of the P3HT:PCBM solar cells by changing the annealing sequence as pre-annealing or post-annealing.

*Authors to whom correspondence should be addressed.

 1533-4880/2013/13/3360/005 doi:10.1166/jnn.2013.7262

2. EXPERIMENTAL DETAILS

2.1. Device Preparation

The device structure of polymer solar cells and their schematic energy band diagram are shown in Figure 1. The patterned indium tin oxide (ITO) substrates with a sheet resistance of 15 Ω/□ were cleaned by using isopropyl alcohol, de-ionized water, acetone, de-ionized water and methanol for 10 min in the named order and were then dried at 120 °C for 2 hours. After that, 10 nm of MoO_3 as a hole extraction layer was deposited under a high-vacuum condition (10^{-6} Torr). On the top of that the P3HT:PCBM film (thickness ~150 nm) was formed by spin-coating the blend solution of P3HT and PCBM with a weight ratio of 1:0.8 in chlorobenzene. Then LiF (0.5 nm) and Al electrodes (100 nm) were evaporated under high-vacuum conditions. We prepared devices with three different annealing conditions, i.e., pristine, pre- and post-annealing: one was thermally treated at 150 °C for 30 min inside the Ar-filled glove box before depositing the LiF/Al electrodes, another was treated after depositing the electrodes, and the other was fabricated without any heat-treatment. The cell size, defined as the overlapped area between ITO and Al electrodes, was 9 mm^2.

2.2. Measurement

The photocurrent–voltage characteristics of the polymer solar cell were measured in the dark and under the air mass 1.5 global (AM 1.5 G) irradiation at 100 mW/cm^2 by using a 300 W solar simulator (Newport 91160A, AM 1.5 G with a KG 5 filter) and a Keithley 237 source measurement unit. The impedance characteristics were measured in the broad frequency range (1000 Hz–10 MHz) by using an impedance analyzer (HP 4192A).

The optical absorption spectra of the as-casted and thermally-annealed P3HT:PCBM films on quartz substrates were taken with a Beckman DU-70 spectrophotometer. We also measured the optical absorption spectra of P3HT:PCBM films at various temperatures from 280 K to 450 K inside the spectrophotometer equipped with a temperature-controlling sample holder. The crystallinity of P3HT:PCBM film was analyzed via X-ray diffractometer (XRD, M18XHF-SR).

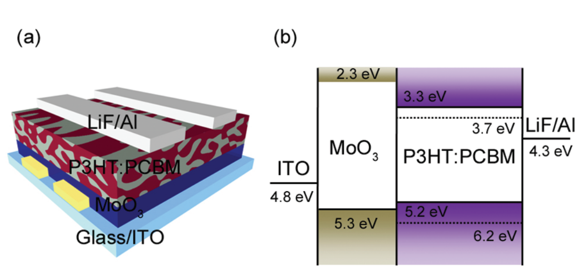

Fig. 1. (a) Structure of the polymer solar cell device: ITO/MoO_3 (10 nm)/P3HT:PCBM (150 nm)/LiF (0.5 nm)/Al (100 nm) and (b) the schematic energy band diagram.

3. RESULTS AND DISCUSSION

Figure 2 shows the optical absorption spectra and XRD patterns of as-casted and thermally-annealed (150 °C) P3HT:PCBM films. As can be seen in Figure 2(a), the optical absorption intensity of the thermally-annealed P3HT:PCBM film increased at the range of 450–650 nm as compared to non-annealed film. This indicates that the oscillator strength for the π–π^* transition of P3HT increases in the thermally-annealed P3HT:PCBM film due to enhanced π-conjugation of the P3HT. From the XRD data shown in Figure 2(b), we can see that the peak intensity around $2\theta = 5.4°$ is greatly increased after the thermal treatment, which is known as the peak of P3HT crystalline.[14] Thus, both data indicate that the thermally-annealed film has improved degree of crystallinity of P3HT domains.

In order to investigate the change of the crystallinity and the degree of π-conjugation of P3HT as a function of temperature in detail, we measured the optical absorption spectra of the pristine and thermally-annealed P3HT:PCBM films with varying the temperature from 280 K to 450 K, and then measured the pristine sample again in the same way after cooling down to the room temperature. We refer to the first measurement of the pristine film with increasing the temperature as ABS_1, the second measurement as ABS_2, and that of thermally-annealed film (at 150 °C) as $ABS_{Annealed}$. In Figure 3(a), the ratio of the peak intensity (at 500 nm) of ABS_1 or ABS_2 to that of $ABS_{Annealed}$ is plotted as a function of temperature so that we can notice how the absorption of pristine film changes

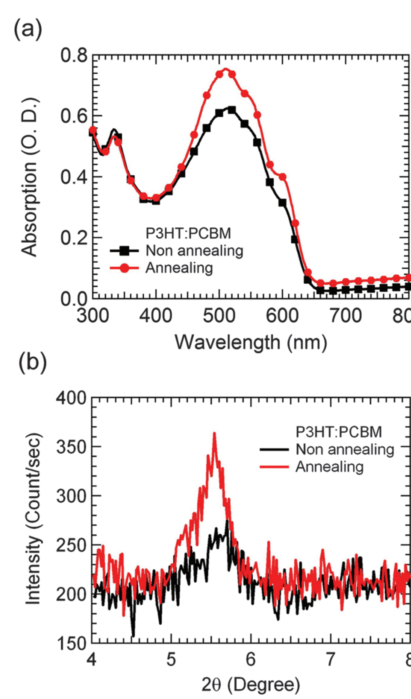

Fig. 2. (a) Absorption spectra and (b) XRD patterns of as-casted and annealed (at 150 °C) P3HT:PCBM films.

RESEARCH ARTICLE

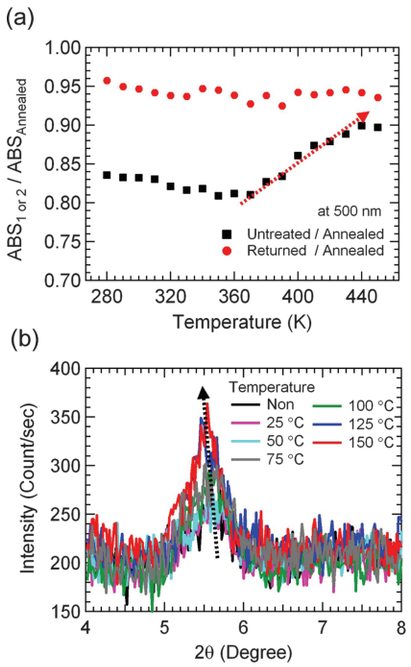

Fig. 3. (a) The ratio of the peak intensity (at 500 nm) of ABS_1 or ABS_2 to that of $ABS_{Annealed}$ as a function of temperature, where the first measurement of the pristine film with increasing the temperatures is ABS_1, the second measurement is ABS_2, and that of annealed film (at 150 °C) is $ABS_{Annealed}$. (b) XRD patterns of as-casted and annealed P3HT:PCBM films with different annealing temperatures (25–150 °C).

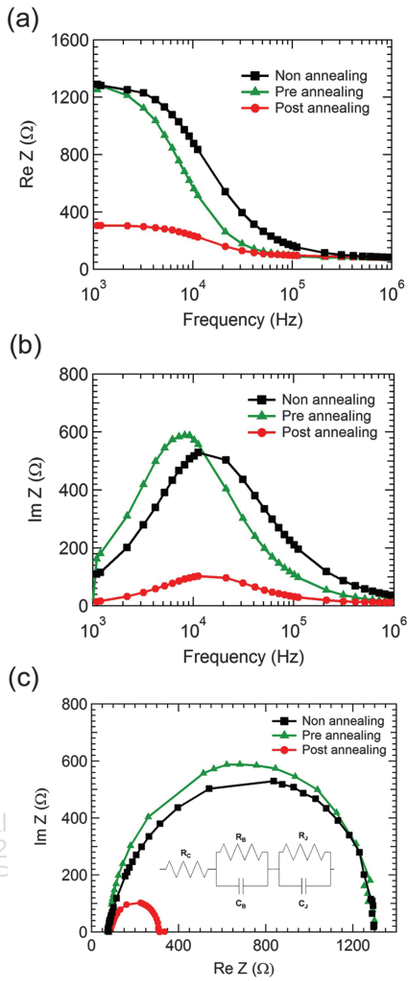

Fig. 4. (a) Frequency dependent real part and (b) imaginary part of the impedance. (c) Cole–Cole plot of pristine, pre-annealed and post-annealed devices (at 150 °C) measured under AM 1.5 G illumination with 100 mW/cm^2. (inset: the equivalent circuit model of the polymer solar cell.)

by temperature compared with that of annealed film. The value of $ABS_1/ABS_{Annealed}$ starts to increase rapidly from around 360 K, indicating that the π-conjugation of the P3HT film starts increasing above ~360 K. However, $ABS_2/ABS_{Annealed}$ is about 0.95 and almost temperature independent since the device is thermally-annealed during the first measurement up to the temperature 150 °C.

The XRD patterns of P3HT:PCBM films with different annealing temperature, shown in Figure 3(b), are consistent with the behavior of optical absorption ($ABS_1/ABS_{Annealed}$). The peak intensity around $2\theta = 5.4°$ is slightly increased after the thermal treatment from 75 °C (~348 K), indicating that the crystallinity of P3HT:PCBM film increases from 75 °C. Consequently, both optical absorption and XRD results indicate that the crystalline order of P3HT:PCBM film increases from ~75 °C, leading to enhanced device performance above ~75 °C, even though the annealing temperature for the optimized formation of donor-accepter interpenetrating networks of P3HT:PCBM film has been known as 150 °C.[15]

As demonstrated above, the thermal annealing process increases light absorption and crystallinity of P3HT:PCBM films, resulting in higher photocurrent. Meanwhile, the sequence of annealing process, i.e., pre-annealing or post-annealing, also affects the performance of solar cells. In order to understand the difference between the devices treated by two annealing processes, we investigated the annealing effect before and after depositing cathode electrodes by analyzing the interface impedance in different conditions.[16, 17]

Figure 4(a) shows the real part of the complex impedance of the pristine, pre- and post-annealed devices (at 150 °C) as a function of frequency under AM 1.5 G solar radiation at 100 mW/cm^2. At low frequency, impedance values of pristine and pre-annealed devices are almost similar but much higher than that of the post-annealed device. The small impedance value in the post-annealed device is attributed to the changes in the interfacial properties between P3HT:PCBM active layer and LiF/Al electrodes. According to the previous report,[15, 18] the surface roughness of post-annealed P3HT:PCBM film is much higher than pristine P3HT:PCBM film. The rough surface increases the interfacial area between P3HT:PCBM active layer and LiF/Al electrodes, resulting in enhanced carrier extraction near the electrodes. Figure 4(b) shows the imaginary

RESEARCH ARTICLE

part of the impedance of pristine, pre- and post-annealed devices versus frequency under illumination. The frequency (ω_c) at which Im(Z) is the maximum provides the junction property of the devices.[17] The ω_c of post-annealed device is higher than that of other devices, which means that the junction resistance of the post-annealed device is lower than other devices. Figure 4(c) shows the Cole–Cole plots, Re(Z) versus Im(Z), of pristine, pre- and post-annealed devices under AM 1.5 G solar radiation at 100 mW/cm^2. The impedance of the device can be modeled as a combination of resistance and capacitance values as follows,[19]

$$Z = R_C + \frac{R_B + j\omega R_B^2 C_B}{1+\omega^2 R_B^2 C_B^2} + \frac{R_J + j\omega R_J^2 C_J}{1+\omega^2 R_J^2 C_J^2} \quad (1)$$

$$Z' = R_C + \frac{R_B}{1+\omega^2 R_B^2 C_B^2} + \frac{R_J}{1+\omega^2 R_J^2 C_J^2} \quad (2)$$

$$Z'' = \frac{\omega R_B^2 C_B}{1+\omega^2 R_B^2 C_B^2} + \frac{\omega R_J^2 C_J}{1+\omega^2 R_J^2 C_J^2} \quad (3)$$

where, R_C is contact resistance, R_B is bulk resistance, and R_J is injection resistance, which are related to the series resistance of ITO, active layer (P3HT:PCBM), and interfaces of MoO_3/P3HT:PCBM and P3HT:PCBM/LiF/Al, respectively.[16, 20] The parameters of impedance analysis for all devices are summarized in Table I. The contact resistances were almost same as 82–101 Ω for all devices because we used same ITO substrates. When the device was thermally annealed after LiF/Al cathode deposition, R_B and R_J decreased from 341.1 Ω and 1206 Ω to 100.5 Ω and 311 Ω, respectively, as compared to the pristine device. In the pre-annealed device, however, R_J increased a little (1338.2 Ω) while R_B decreased by half (147.5 Ω) as compared with the pristine device. These results indicate that the properties of interface (i.e., between P3HT:PCBM and LiF/Al) in the post-annealed device is mainly different from the pre-annealed device since we can consider the interface of MoO_3/P3HT:PCBM is similar for all devices owing to their common structure and procedures.

Figure 5(a) shows the current density–voltage characteristics of pristine, pre- and post-annealed devices, which were measured under AM 1.5 G solar radiation at 100 mW/cm^2. The solar cell parameters in terms of the short-circuit current (J_{SC}), open-circuit voltage (V_{OC}), fill factor (FF), and PCE are summarized in Table II. When the device was thermally annealed, the fill factor increased greatly from 51.70% to 60.08 or 62.87% regardless of the annealing method. However, in case of the pre-annealed device, J_{SC} was only half of that in the post-annealed device and even lower than the non-annealed device. These results can be supported by the lower injection resistance in the post-annealed device compared to the other devices as shown in Figure 4(c). Figure 5(b) shows that J_{SC} follows a power law ($J_{SC} = P_{light}^{\alpha}$), where P_{light} is the light intensity and α is the exponent which is correlated to the recombination processes in organic solar cells.[21] It is known that the exponent $\alpha = 1$ for the monomolecular recombination process while $\alpha = 0.5$ for the bimolecular recombination process. In our case, the post-annealed device has the value α of 0.887, which is slightly higher than those of the pre-annealed ($\alpha = 0.874$) and pristine devices ($\alpha = 0.871$). These results signify that recombination loss of the post-annealed device is relatively smaller than that of the others.

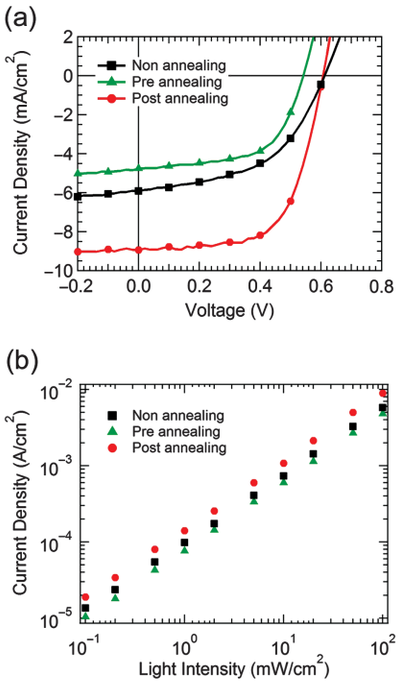

Fig. 5. (a) Current density–voltage characteristics of the polymer solar cells. (b) Double-logarithmic representation of the short-circuit current density as a function of light intensity (1–100 mW/cm^2) for the pristine, pre-annealed and post annealed devices (at 150 °C) measured under AM 1.5 G illumination with 100 mW/cm^2.

Table I. The contact, bulk, and injection resistance values calculated from the impedance spectroscopy results of the pristine, pre- and post-annealed solar cell devices, which were measured under AM 1.5 G illumination with 100 mW/cm^2.

	R_C (Ω)	R_B (Ω)	R_J (Ω)
Non-annealing	101.1	341.1	1206.1
Pre-annealing	84.1	147.5	1338.2
Post-annealing	82.0	100.5	311.3

Table II. Device performance of the solar cells with different annealing sequences, which were measured under AM 1.5 G illumination with 100 mW/cm^2.

	J_{SC} (mA/cm^2)	V_{OC} (V)	FF (%)	PCE (%)
Non-annealing	5.79	0.61	51.70	1.86
Pre-annealing	4.76	0.54	60.03	1.55
Post-annealing	8.93	0.60	62.87	3.40

RESEARCH ARTICLE

4. CONCLUSION

In conclusion, we have investigated the device performance of polymer solar cells based on P3HT:PCBM with different annealing sequences. From the optical absorption and XRD results, the crystallinity of P3HT:PCBM starts from ~75 °C, even though the optimal annealing temperature has been known as 150 °C. Compared with the pre-annealed device, the post-annealed device exhibited much higher performances in terms of the J_{SC}, V_{OC}, FF as well as the PCE, which was mainly attributed to the increase of J_{SC}. To explain the reason for the J_{SC} enhancement, impedance properties of all devices were measured and modeled with the combination of resistance and capacitance. From impedance results, we could know that the injection resistance of the post-annealed device was lower than that of the pristine and pre-annealed devices. Accordingly, the post-annealed device has improved charge transport and extraction within P3HT:PCBM film, resulting in the improve power conversion efficiency.

Acknowledgment: This work was supported by the Human Resources Development of the Korea Institute of Energy Technology Evaluation and Planning (KETEP) grant funded by the Korea government Ministry of Knowledge Economy (No. 20124010203170).

References and Notes

1. P. Schilinsky, C. Waldauf, and C. J. Brabec, *Adv. Funct. Mater.* 16, 1669 (**2006**).
2. S. E. Shaheen, R. Radspinner, N. Peyghambarian, and G. E. Jabbour, *Appl. Phys. Lett.* 79, 2996 (**2001**).
3. C. J. Brabec, N. S. Sariciftci, and J. C. Hummelen, *Adv. Funct. Mater.* 11, 15 (**2001**).
4. J. Hou, H.-Y. Chen, S. Zhang, R. I. Chen, Y. Yang, Y. Wu, and G. Li, *J. Am. Chem. Soc.* 131, 15586 (**2009**).
5. G. Zhao, Y. He, and Y. Li, *Adv. Mater.* 22, 4355 (**2010**).
6. H.-Y. Chen, J. Hou, S. Zhang, Y. Liang, G. Yang, Y. Yang, L. Yu, Y. Wu, and G. Li, *Nat. Photon.* 3, 649 (**2009**).
7. M. C. Scharber, D. Mühlbacher, M. Koppe, P. Denk, C. Waldauf, A. J. Heeger, and C. J. Brabec, *Adv. Mater.* 18, 789 (**2010**).
8. T. J. Savenije, J. E. Kroeze, X. Yang, and J. Loos, *Adv. Funct. Mater.* 15, 1260 (**2005**).
9. A. Orimo, K. Masuda, S. Honda, H. Benten, S. Ito, H. Ohkita, and H. Tsuji, *Appl. Phys. Lett.* 96, 043305 (**2010**).
10. D. Chen, A. Nakahara, D. Wei, D. Nordlund, and T. P. Russell, *Nano Lett.* 11, 561 (**2011**).
11. M.-S. Kim, B.-G. Kim, and J. Kim, *ACS Appl. Mater. Interfaces.* 1, 1264 (**2009**).
12. W.-H. Tseng, M.-H. Chen, J.-Y. Wang, C.-T. Tseng, H. Lo, P.-S. Wang, and C.-I. Wu, *Sol. Energy Mater. Sol. Cells* 95, 3424 (**2011**).
13. G. Li, V. Shrotriya, Y. Yao, and Y. Yang, *J. Appl. Phys.* 98, 043704 (**2005**).
14. T. Erb, U. Zhokhavets, G. Gobsch, S. Raleva, B. Stühn, P. Schilinsky, C. Waldauf, and C. J. Brabec, *Adv. Funct. Mater.* 15, 1193 (**2005**).
15. W. Ma, C. Yang, X. Gong, K. Lee, and A. J. Heeger, *Adv. Funct. Mater*. 15, 1617 (**2005**).
16. G.-H. Kim, H.-K. Song, and J. Y. Kim, *Sol. Energy Mater. Sol. Cells* 95, 1119 (**2011**).
17. C. K. Suman, S. Noh, S. Kim, S. D. Lee, and C. Lee, *J. Korean Phys. Soc*. 53, 3278 (**2008**).
18. H. Kim, W.-W. So, and S.-J. Moon, *Sol. Energy Mater. Sol. Cells.* 91, 581 (**2007**).
19. M. Meier, S. Karg, and W. Riess, *J. Appl. Phys.* 82, 1961 (**1997**).
20. C. Melzer, V. V. Krasnikov, and G. Hadziioannou, *Appl. Phys. Lett.* 82, 3101 (**2003**).
21. P. Schilinsky, C. Waldauf, and C. J. Barbec, *Appl. Phys. Lett.* 81, 3885 (**2002**).

Received: 5 November 2011. Accepted: 20 April 2012.

RESEARCH ARTICLE